Stiffening Effects on the Shear Behaviour of Single Perforated Lean Duplex Stainless Steel (LDSS) Rectangular Hollow Beams

Sonu J.K and Konjengbam Darunkumar Singh

Department of Civil Engineering, Indian Institute of Technology Guwahati, India

Abstract

In this study, a numerical investigation on the effects of various parameters of the inclined flat stiffeners e.g. cross-sectional dimensions (length, l_s; width, b_s; thickness, t_s) on the shear characteristic of single circular perforated short span (a/h_w= 1; a = shear span, h_w= web height) lean duplex stainless steel (LDSS) rectangular hollow beam is presented. Based on the study it has been observed that the rate of increase in shear capacity (V_u/V_y) increases with increasing l_s for higher values of t_s (e.g. $t_s/t_w \geq 3$). It is also seen that it is possible to achieve the strength of unperforated beam, with larger stiffener length and thickness. However, no significant change in the value of shear capacity for increase in stiffener width for short stiffener (l_s/d_o = 1.00), could be observed.

Keywords

Rectangular hollow LDSS tubular beam, Web perforation, Shear behaviour, Lean duplex stainless steel beam, Stiffener.

1 Introduction

In the recent years, a gradual increase in the use of stainless steel structural members in the construction industry has been observed, especially for exposed architectural elements. Although it is well known that, stainless steel, can provide improved corrosion resistance. Their uses are limited, mainly because of their relatively high initial cost (e.g. Mann, 1993; Gardner, 2005; Ashraf et. al., 2006; Theofanous and Gardner, 2010; Saliba and Gardner, 2013; Estrada et. al., 2007). Of late, a relatively new and promising grade of stainless steel known popularly as Lean Duplex Stainless Steel, LDSS (LDX 2101 / EN 1.4162 / UNS 32101) has been introduced, with attractive properties as reduced initial material cost (via a cut down in nickel content), improved strength, fracture toughness properties (e.g. Theofanous and Gardner, 2010, Saliba and Gardner, 2013), acceptable weldability (Nilsson et. al., 2008), high temperature properties (Gardner et. al., 2010), etc. This has led to an increase in the research interests on LDSS structural members (e.g. Theofanous and Gardner, 2010; Saliba and Gardner, 2013; Huang and Young, 2013, 2014).As a continuous effort in gaining further understanding on LDSS members, recently, shear characteristics of LDSS rectangular hollow beams: both unperforated and perforated have been reported by the authors (Sonu and Singh, 2017a, 2017b). Perforations / openings/ cut outs on beam webs can provide helpful ways to accommodate building services ducts; secondary constructional elements; to increase strength/weight ratio; and to decrease the stress transfer to beam-column joint; for inspection, repair and maintenance work, etc. (e.g. Hagen et. al., 2009; Feng and Young, 2015; Lagaroset. al., 2008). As such perforations, can have detrimental effects on structural elements, it become necessary to explore the ways to mitigate their effects. In the literature, several types of stiffeners (e.g. ring, horizontal, transverse, sleeves, doubler plate stiffeners) were employed to augment load (shear, compression etc.) capacity of open webs/plate perforated with circular / rectangular holes (see e.g. Narayanan and Der-Avanessian, 1984; Keerthan and Mahendran, 2013; Hamoodi and Gabar, 2013; Hagen et. al., 2009; Kim et. al., 2015). It may be noted that such studies were mainly on open sections e.g. plates, I-sections etc. Types of stiffeners used in members subjected to shear loading are doubling plate (Keerthan and Mahendran, 2013; Kim et.al, 2015); ring (Keerthan and Mahendran, 2013; Hamoodi and Gabar, 2013, Narayanan and Der-Avanessian, 1984; Kim et.al., 2015); vertical and horizontal, inclined (Cheng and Li, 2012) stiffeners. In this study, such studies are extended to assess the shear behaviour of stiffened single perforated LDSS rectangular hollow beam (i.e. closed section), using FE analysis approach considering diagonal / inclined. More specifically, in this paper, the effect of variation in cross-sectional dimensions (or slenderness) e.g. width (b_s), thickness (t_s) and length (l_s) of inclined (or diagonal) stiffener pattern is investigated. The results of the FE analyses are presented in the form of variations in shear capacity (V_u/V_y) with respect to normalised parameters like l_s/d_o, b_s/h_w (for various values of t_s/t_w), mid-span deformation (δ), deformation shapes etc.

2 Numerical (FE) Modelling

2.1 General

The FE modelling procedure (e.g. meshing, boundary conditions, imperfection seeding, material modelling etc.) followed in this study is similar to those described in studies of Theofanous and Gardner (2010), Sonu and Singh (2017a, 2017b) for LDSS rectangular beams and Saliba and Gardner (2013). Geometry and FE mesh used for the stiffeners are presented in the following subsections.

2.2 Geometry and boundary conditions

Figure 1 shows the schematic representation for a typical geometry (Figure 1a & 1b), FE mesh (Figure 1c) and boundary conditions (Figure 1d) considered. The various fixed cross-sectional parameters were h_w = 600 mm, a =

600 mm, w_f = 200 mm, t_f = 10 mm, t_w = 2 mm, such that a/h_w = 1.0, h_w/t_w = 300 and t_f/t_w = 5 where h_w, t_w, w_f, t_f and a are height of web, web thickness, flange width, flange thickness and shear span respectively. Note that hw and wf are the internal and outer dimensions respectively of the beam. The in-plane deformation of the beam is constrained at both ends and mid-span via kinematic coupling (Theofanouset. al., 2009; Theofanous and Gardner, 2010) available in Abaqus (2009). Constraining of the nodes at the sections of mid-span (i.e. at the section where the external displacement is applied) and end supports have been artificially done to avoid local buckling due to the externally applied displacement and support reactions, and thus ensuring rigid post conditions, both at the mid-span and end supports shown in Figure 1(c). In order to get constant shear along the span of the beam (shear span is half the beam length, i.e. a = L/2), beam is simply supported at both the ends (one end is hinge and other is roller supported), and point displacement is applied statically at the mid-span of the beam as shown in Figure 1(d).A centrally located perforation with moderately large diameter, do = 300 mm (d_o/h_w = 0.5) was chosen as the benchmark perforated beam upon which the effect of stiffener is studied. It may be noted that the reduction maximum in the shear capacity for the case of do/hw = 0.5 was seen to be about 26% as compared to the unperforated case (see Sonu and Singh, 2017b). Single perforation is located at the centre of the web at single shear span. As mentioned above, in this study, inclined / diagonal stiffener (IS) was considered (see Figure 2a). Two parallel inclined stiffeners of equal length located at opposite sides of perforation were considered. Stiffener with flat (or rectangular) cross-section were considered to assess cross-sectional shape effect (see Figure 2).

The values of length (l_s), breadth (b_s) and thickness (t_s) of the stiffeners adopted in the FE analyses ranged from 300-515 mm (or l_s/d_o = 1.00-1.75, where d_o = diameter of opening), 24-72 mm (or b_s/h_w = 0.04-0.12) and 2 &14 mm (or t_s/t_w = 1-7). A 10 mm clearance(s/t_w = 5, where s is the distance between edge of opening to stiffener edge) of the stiffeners from the edge of the perforation has been maintained, such that the stiffeners are separated by an additional 20 mm (i.e. 2 × 10 mm) in addition to the perforation size (or perforation diameter, d_o). The clearance was assumed to avoid the stiffener being too close to the perforation edge so that welding can be done at ease (e.g. Hagen (2005) assumed s/t_w = ~ 0.6-1.2 i.e., 10-20 mm; Cheng and Zhao (2010) have taken the s/t_w = 0.5). The stiffeners (IS) were provided perpendicular to the diagonal of the perforated web (resulting in perpendicular to the tension band, as seen in Figure 6b, P1); in the case (i.e. a/h_w = 1), it is at 45o to the longitudinal axis of the beam. Further, the maximum length of stiffener (l_s) was chosen so that the outer dimensions of the stiffeners were limited to the inner edge of the flanges.

2.3 Finite element mesh

Typical FE mesh of the stiffened perforated beam is shown in Figure 1c (d_o/h_w = 0.50; a/h_w = 1.0). Except for the region surrounding the perforation, similar global square mesh size (~18–25 mm) arrived through mesh convergence study for unperforated beam (see Sonu and Singh, 2017a, 2017b) are again used to model the geometry of the beam. In order to capture the local stress near the perforation edge, a widely reported fan-type mesh (see e.g. Ridley-Ellis, 2000; Hagen et.al, 2009; Hagen, 2005; Liu and Chung, 2003; Paik, 2007; Pellegrino et.al, 2009; Bowmick, 2014) pattern adjoining the circular perforation has been adopted. The fan-type mesh around the perforation is confined to a square of sides ~$1.7d_o$ – $4d_o$ (achieved through 'partitioning' in Abaqus, 2009) number of elements along the edge of the perforation is equal to those of elements located at the edge of the square region surrounding the fan-type mesh. Inside the partitioned square region, the number of elements radiating from perforation edge is in the range ~8–10. A uniform mesh size was seeded along the radial direction inside the partitioned square region. Studies using biased mesh (with mesh size getting finer towards the perforation edge) did not significantly alter the results, hence only uniform radial meshing was adopted. The total number of S4R elements adopted are in the range ~6500–7000 for the beams without stiffener. The aforementioned mesh configuration is found to be optimum and sufficiently fine enough, and are arrived at after performing mesh convergence study through linear elastic eigen-value buckling analysis.

Stiffeners were also meshed with similar elements i.e. S4R elements (with aspect ratio ~1), except that relatively finer meshes (or smaller elements) were adopted, since the stiffener geometry is smaller in comparison to the main beam. A minimum of 10 S4R elements were adopted along the length of the stiffener in order to capture the interaction of stresses between the perforated web and stiffeners, based on mesh convergence study. The stiffeners were modelled separately using a uniform mesh and then tied to the perforated web through 'tie' option available in Abaqus (2009). This makes it possible to mesh both the web and stiffener, without much concern on the node location compatibility at the junction. The total number of elements in a stiffener ranges from 50–200, depending on their geometry.

2.4 Local geometric imperfection

Geometrical imperfections arising during fabrication, production, transportation etc. are the undulations on geometry compared to perfect ones; it exists in actual structures and affects the structural performance. In the present study, only local imperfections are incorporated in the analysis by considering the lowest eigen mode from linear elastic eigen-value buckling analysis (e.g. Theofanous and Gardner, 2010; Saliba and Gardner, 2013). The imperfection amplitude provided by Dawson and Walker (1972) model (Equation 1) which has been employed by Gardner and Nethercot (2004) for stainless steel, is applied to the lowest eigen mode to perturb the actual geometry of the beam for subsequent non-linear analyses.

$$\omega_o / t = 0.023\left(\frac{\sigma_{0.2}}{\sigma_{cr}}\right) \qquad (1)$$

where $\sigma_{0.2}$ and σ_{cr} are the 0.2 % proof stress and elastic critical buckling stress (in this case, obtained via linear elastic eigen-value analysis using subspace iteration method, using Abaqus, 2009) of plated elements respectively.

3 Material Modelling

The material properties (Tables 1) for the LDSS material used in the present study is based on the experimental study conducted on LDSS hollow beams by Theofanous and Gardner (2010). As per EN 10088-4 (2009), an ultimate tensile strength ranging from 700–900 MPa and a minimum 0.2% proof stress ($\sigma_{0.2}$) of 530 MPa can be associated with LDSS Grade EN 1.4162. A modified two stage (Equations 2 and 3) compound Ramberg-Osgood (1943) proposed by Gardner and Ashraf (2006) for stainless steel material has been adopted for the non-linear stress-strain curve used in the present FE analyses. Equation 2 represents the Ramberg-Osgood (1943) model for $\sigma \leq \sigma_{0.2}$ ($\sigma_{0.2}$is the 0.2% proof stress) and is reported in the literature to provide good accord with stress strain curve obtained from experiments for steel up to $\sigma_{0.2}$. For strains exceeding $\varepsilon_{t0.2}$ (total strains at $\sigma_{0.2}$), Ramberg-Osgood model is known to give higher values of stress values as compared to that of experimental data, and hence a modified version has been suggested by Gardner and Ashraf (2006) (see Equation 3). Using the full expression (both Equations 2 and 3) for stress-strain behavior it has been shown by Gardner and Ashraf (2006) that their model could provide reasonably good comparison for stainless steel in both compression and tension loading cases. In the Abaqus model, the two-stage non-linear stress strain model given by Equations 2 and 3 are approximated by a piecewise-linear stress-strain curve, taken due care to insert enough points where the curvature is sharper. The values of E_o for both compression (above neutral axis) and tensile (below neutral axis) parts are given in Table 1 (from Theofanous and Gardner, 2010). Poisson's ratio was taken as 0.3. Figure 3 shows the schematic stress-strain diagram of LDSS of grade EN 1.4162 used to input in the FE model after the conversion of engineering stress-strain to true plastic stress (σ_{true}^{pl})-strain (ε_{true}^{pl}) using the Equations 4 and 5.

$$\varepsilon = \frac{\sigma}{E_o} + K\left(\frac{\sigma}{\sigma_{0.2}}\right)^n \tag{2}$$

$$\varepsilon = \left(\frac{\sigma - \sigma_{0.2}}{E_{0.2}}\right) + \left(\varepsilon_{t1.0} - \varepsilon_{t0.2} - \frac{\sigma_{1.0} - \sigma_{0.2}}{E_{0.2}}\right) \times \left(\frac{\sigma - \sigma_{0.2}}{\sigma_{1.0} - \sigma_{0.2}}\right)^{n'_{0.2,1.0}} + \varepsilon_{t0.2} \tag{3}$$

$$\sigma_{true} = \sigma_{norm}(1 + \varepsilon_{norm}) \tag{4}$$

$$\varepsilon_{true}^{pl} = \ln(1 + \varepsilon_{norm}) - \frac{\sigma_{true}}{E_0} \tag{5}$$

where σ_{norm} and ε_{norm} are engineering stress and strain respectively.

The conversion of the nominal static stress-strain curve to true stress and true strain curve was considered necessary as the post-buckling analysis involves significant in elastic strains (e.g. Theofanous and Gardner, 2009; Patton and Singh, 2012). Further, modified RIKS method (Riks,1979) available in Abaqus (2009) has been used for the non-linear analysis to obtain structural behaviors such as full shear and mid-span deflection response of the beam accurately.

4 Validation of Finite Element Model

Before proceeding with the parametric study, it becomes imperative to validate (or calibrate) the FE modeling procedures with known 'reliable' experimental result(s) to establish the accuracy and hence confidence in the modeling. Hence, in this work, the present FE modeling approach has been validated against representative experimental results reported by Theofanous and Gardner (2010) and Saliba and Gardener (2013), for tests on LDSS square hollow beam and LDSS plate girders respectively. This particular experimental has been so chosen considering the similarities in cross-sectional properties and loading (3-point loading) conditions with the geometry, loading patterns and failure pattern of the specimens adopted herein. The material data of the benchmark specimen as well as geometry is shown in Tables 1, 2 & 3. No residual stress distribution (note that residual stress was expected as the specimen was cold worked or formed) is explicitly considered in the present modeling, as experimental material properties has inherent effect of residual stress (Theofanous and Gardner, 2010, Saliba and Gardner, 2013). Comparison of experimental and FE are shown in Figures 4 & 5. From Figures 4 & 5, it can be readily observed that the present FE procedure is able to capture the key experimental behavior *viz.*, M_u, V_u (ultimate moment capacity, shear capacity), very well, in addition to the overall curve pattern. Hence, it can be assumed that the present FE modeling approach is expected to predict the structural LDSS beam behaviour with a reasonable confidence. It may also be noted that the comparison (or validation) presented in this work is due to the lack of experimental results stiffened perforated LDSS hollow sections subjected to shear loading. Thus, in the following present study, such well established modeling shell FE modeling procedures which are employed widely in the literature is for modeling thin-walled metallic structures / members is considered.

4.1 Parametric study

In the parametric study, the effect of stiffeners dimensions (l_s, b_s, t_s) on the shear characteristic of single circular perforated short span (a/h_w = 1) LDSS rectangular hollow beam was investigated, for the range of parameters mentioned in Section 2.2. The results are presented in the form of i) variation of shear with mid-span transverse deformation (V/V_y vs δ), von-Mises stress contours, and variation of shear capacity (V_u/V_y).

4.2 Results and discussion

The effect of the inclined stiffener on the shear behavior*viz*., shear capacity and deformed shapes are presented in terms of variation in stiffener lengths (l_s) and breadth (b_s). The results for perforated (without stiffeners) and unperforated beams are also presented for comparison.

Effect of stiffener length (l_s)

Variation of V/V_y with δ (along with von-Mises contour plots) for b_w = 24 mm (or b_w/h_w= 0.04) are shown in Figures 6 and 7 for thin (t_s = 2 mm or t_s/t_w = 1) and thick (t_s = 14 mm or t_s/t_w = 7) stiffeners respectively. In Figures 6a and 7a, the results are presented for l_s = 300–525 mm (or l_s/d_o = 1.00–1.75 i.e. 75% increase in l_s from 300 mm). It can be seen from Figure 6a, there is no significant change in both the shear capacity (V_u/V_y or V_{RF}/V_y) or the shape of the V/V_y vs δ profile, for the thin stiffeners considered. An increase of about 2% in V_u/V_y can be observed when l_s is increased by 75%. The enhancement in V_u/V_y for the stiffened beam in comparison to the perforated beam is about ~1.5–3.6%. Figure 6b, shows the von-Mises contour plot at V_u, V_{RF} and post V_{RF} shear values, for unperforated (S1, S2, S3), perforated (P1, P2 and P3), and stiffened beams (inset L1, L2 and L3 for l_s/d_o = 1; inset H1, H2 and H3 for l_s/d_o = 1.75). It can be seen that there is little variation in von-Mises stress contour plot and deformed shapes for l_s/d_o = 1.00 and 1.75 (see L1, L2, L3 and H1, H2, H3). This may be related to the relatively thin section (t_s/t_w = 1) considered. It is also seen that due to the presence of stiffeners, the local corrugated (accompanied by both inward and outward buckling) buckling of perforation edges (mostly along the tension band; see inset figure P1 in Figure 6b) is now changed to outward local buckling, at V_u. The outward local buckling of the stiffened web (inset L1 and H1 figures in Figure 6b), may be related to the weaker cross-sectional slenderness (owing to thinner section). Very similar post-V_u failure modes (i.e. formation of plastic hinge in the compression flange, stress distribution pattern in the vicinity of the perforation) are also seen for both the short and long values of l_s; this observation also agrees with the similar values of δ_{RF} as seen in Figure 6a.

The effect of thick stiffener (t_s/t_w = 7; or t_s = 14 mm) is shown in Figure 7 (l_s/d_o= 1.00–1.75, b_w/h_w = 0.04). From Figure 7a, a significant enhancement in the shear capacity of the stiffened beam can be seen when the value of l_s/d_o is increased from 1.00–1.75 (i.e. as the stiffener gets thicker). The increase in V_u/V_y is ~2.8, 6, and 21% for l_s/d_o = 1.25, 1.5 and 1.75 respectively, in comparison to l_s/d_o = 1.0. For, the smallest length considered i.e. l_s/d_o =1.00, the value of V_u/V_y is found to be higher by ~9% compared to the perforated case. When l_s/d_o = 1.75, the unperforated shear capacity is nearly recovered. It may be noted that the value of δ_{RF} for the longest stiffener length considered (i.e. l_s/d_o = 1.75) is about ~25% shorter as compared to that corresponding to l_s/d_o = 1.00 i.e. the onset of rapid-falling curve occurs much earlier when the thickness of the stiffener is sufficiently large enough. Von-Mises contour plot corresponding to l_s/d_o = 1.0 and 1.75 are shown in Figure 7b. It can be observed that due to the presence of the thick stiffeners, highly stressed Von-Mises stress near the perforation is relatively distributed over a larger area, at V_u (see inset figures L1 and H1 in Figure 7b). Again, corrugated local buckling at the perforated edge of the unstiffened web, is prevented due to the stiffening effect. But unlike in the case with thin stiffeners, the outward buckling of the stiffened web is visibly reduced (see L1 and H1 in Figure 7b), when thick stiffeners are used. It may be noted that for the longest stiffener (i.e. l_s/d_o = 1.75), the formation of plastic hinge at the compression flange is now shifted towards the unperforated side (see H2), unlike the case for shorter stiffener (see L1 and L2). This may be because, due to the thick elongated stiffener, significant improvement in the load capacity of the perforated span may have achieved. The effect of l_s on the shear capacity is plotted in the form of V_u/V_y vs l_s/d_o, for thickness, t_s/t_w = 1-7 (or t_s = 2 &14 mm) in Figure 8. Shear capacity increased with increase in stiffener thickness (t_s/t_w = 1 & 7) in a nonlinear trend. It can be seen that, for higher thicknesses, the rate of increase in V_u/V_y increases with increasing l_s/d_o, thus suggesting that the role of stiffener thickness in enhancing the shear capacity becomes more effective at longer length (l_s). For the longest and thickest stiffener (l_s/d_o = 1.75 &t_s/t_w = 7), the stiffened perforated beam has already achieved the shear capacity of unperforated beam.

Effect of stiffener breadth (b_s)

The effect of stiffener breadth (b_s) is presented in the form of variation of V/V_y with δ, von-Mises contour plots, and V_u/V_y with b_w/h_w, for two cases *viz*., short (l_s/d_o = 1) and long (l_s/d_o = 1.75) stiffeners in Figures 9–11 and 12–14 respectively. Variation of V_u/V_y with δ and von-Mises contour plots are shown for thin (t_s/t_w = 1) and thick (t_s/t_w = 7) for short stiffener (l_s/d_o = 1) in Figures 9 and 10 respectively, for b_s ranging from 24–60 mm (or b_s/h_w = 0.04–0.10). Moreover, it can be seen from Figures 9 and 10 that it is not able to regain the unperforated shear capacity even after an increase of 150% in b_s from 24 mm. For both the thin and thick stiffeners, the enhancement in V_u/V_y is ~8.8% as compared to the unstiffened beam. It is also seen that the von-Mises stress distribution in the stiffened perforated web is not noticeably changed for the change in b_s (see L1, H1 in Figures 9 and 10). Figure 11 shows the variation of V_u/V_y with b_s/h_w for t_s/t_w = 1–7. It can be seen that, there is no significant change in the value of V_u/V_y for b_s/b_w ranging from 0.04–0.10, for the thicknesses considered, suggesting that there is not much benefit in increasing the cross-sectional dimension (in terms of b_s and t_s) for short stiffeners (l_s/d_o = 1.0). In the case of long stiffeners (l_s/d_o = 1.75), an improved enhancement in V_u/V_y can be seen even for thin stiffeners; an increase of ~19% in V_u/V_y as compared to non stiffened case, can be observed for b_s/h_w = 0.10 (or b_s = 60 mm) as shown in Figure 12a. Whereas for thick stiffeners (t_s/t_w = 7), almost full strength of the unperforated beam could be achieved at lower b_s (= 0.04). A comparison of the von-Mises contour plots between thin (Figure 12b) and thick (Figure 13b) stiffeners for longer stiffeners shows that due to sufficiently improved shear capacity has resulted in the occurrence of plastic hinge formation at the compression flange being shifted towards the unperforated span (L2 and H2 in Figure 13b), with stress relaxation in the stiffened webs. Variation of V_u/V_y with b_s/h_w for long stiffeners (l_s/d_o = 1.75) is shown in Figure 14, for t_s/t_w = 1–7. It can be seen that, uperforated shear capacity has been achieved at for all the stiffener widths (b_s/h_w = 0.04, 0.06, 0.08& 0.10) for t_s/t_w = 7, whereas it could not be attained for the thin stiffener (t_s/t_w = 1).

5 Conclusions

FE studies on shear behaviour of single perforated LDSS rectangular hollow beam stiffened with inclined stiffeners have been presented considering cross-sectional dimensions (or slenderness) e.g. length (l_s),width (b_s) and thickness (t_s). Based on the present study, it has been observed that the rate of increase in shear capacity (V_u/V_y) increases with increasing stiffener length. It is also seen that it is possible to achieve the strength of unperforated beam, with larger stiffener length and thickness, e.g. for the longest and thickest stiffener (l_s/d_o = 1.75 &t_s/t_w = 7) considered, the stiffened perforated beam has achieved the shear capacity of unperforated beam. It is found that, there is no significant change in the value of shear capacity for increase in stiffener width, suggesting that there is not much benefit in increasing the cross-sectional dimension (in terms of b_s and t_s) for short length stiffeners (l_s/d_o = 1.0). In the case of long stiffeners, an improved enhancement in shear capacity can be seen even for thin stiffeners e.g. an increase of ~19% in V_u/V_y as compared to non stiffened case, can be observed for b_s/h_w = 0.10 (or b_s = 60 mm). Whereas for thick stiffeners (e.g. t_s/t_w = 7), almost full strength of the unperforated beam could be achieved at lower b_s (e.g. b_s = 0.04).

6 Figures

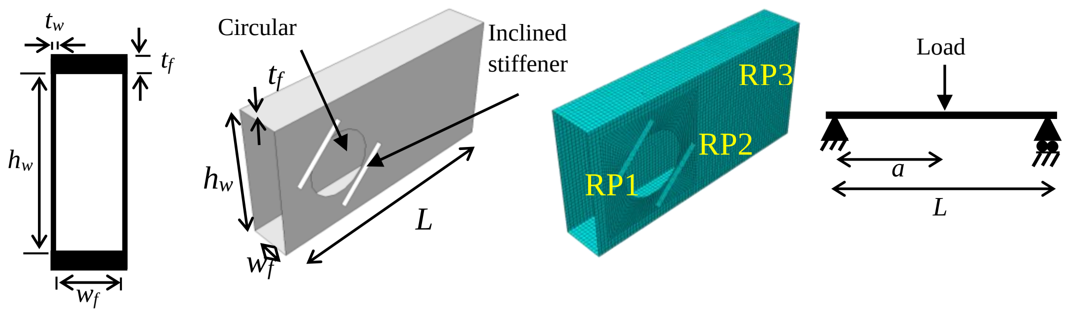

(a) **(b)** **(c)** **(d)**

Fig. 1 (a) Geometry (b) stiffener (c) Mesh (d) Loading and support condition

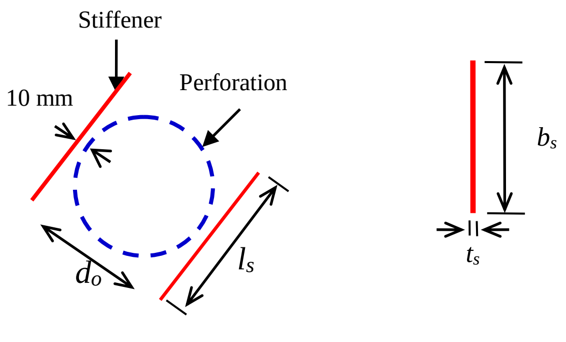

(a) Pattern **(b) Cross-section**

Fig. 2 Schematic diagram of straight Inclined Stiffener (IS).

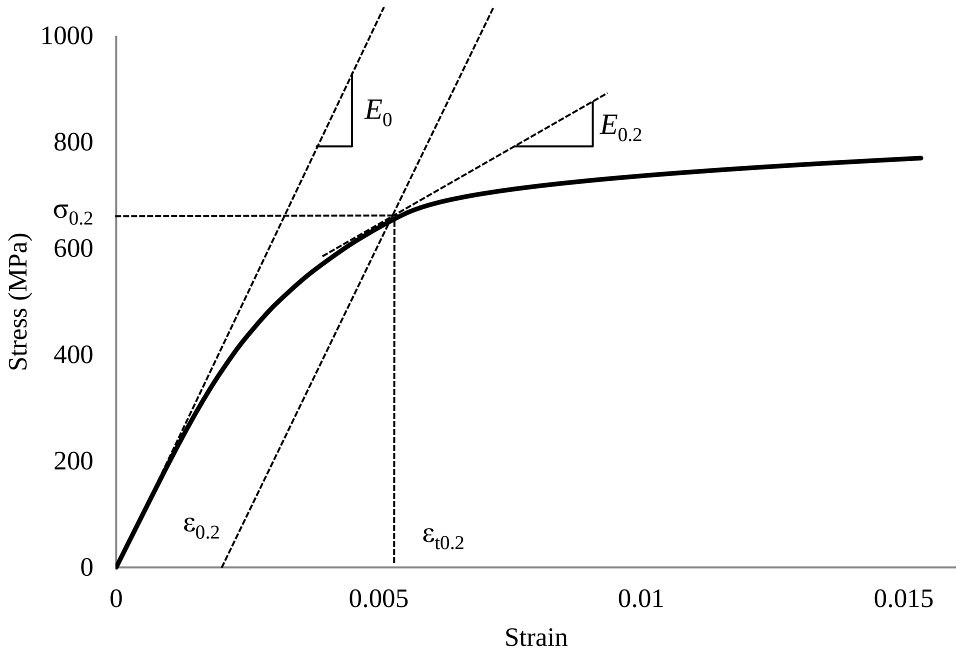

Fig. 3 Stress-strain curve of LDSS material Grade EN 1.4162 (Gardner & Ashraf, 2006)

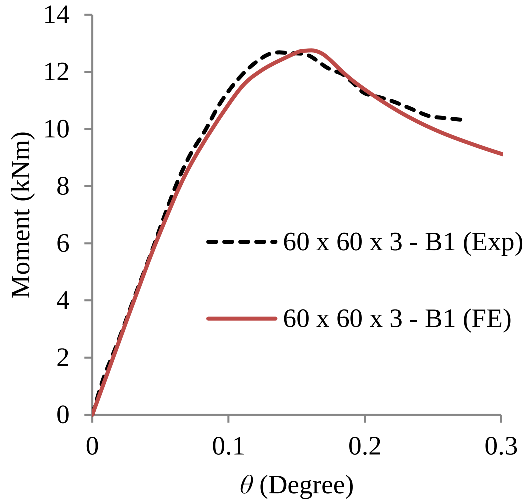

(a)

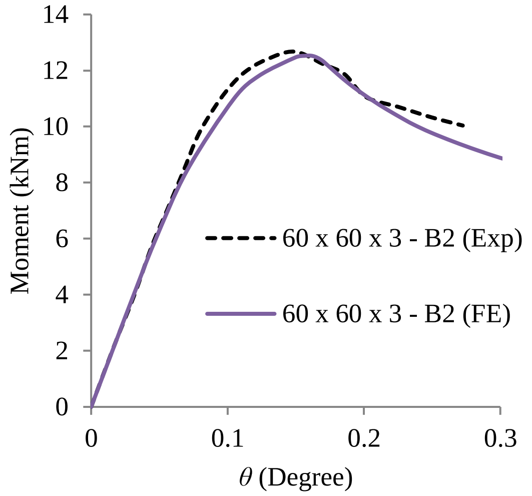

(b)

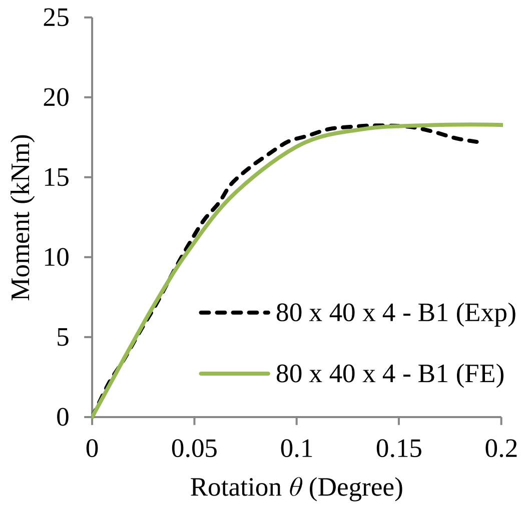

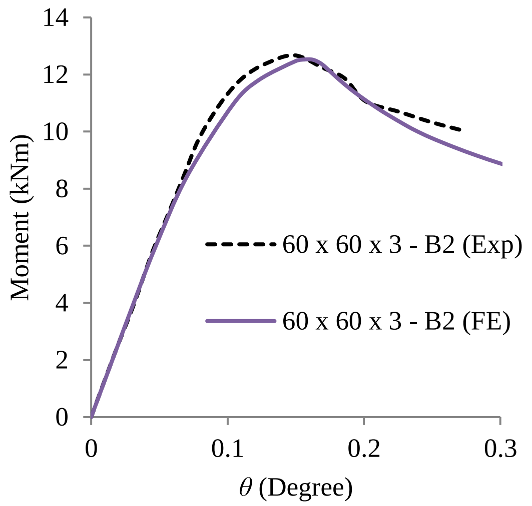

(c)

(d)

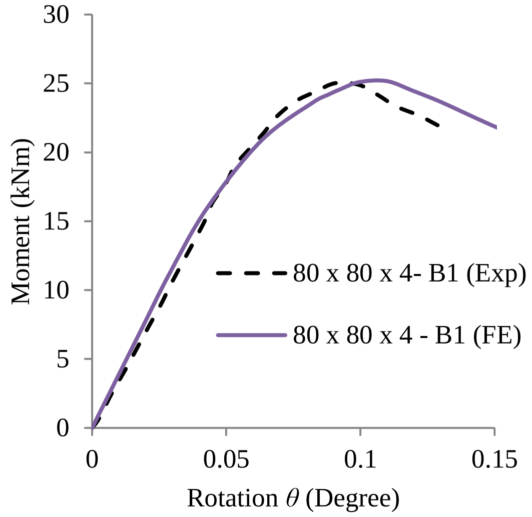

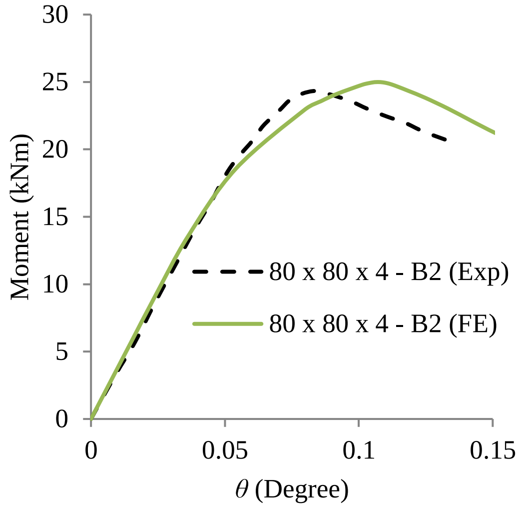

(e)

(f)

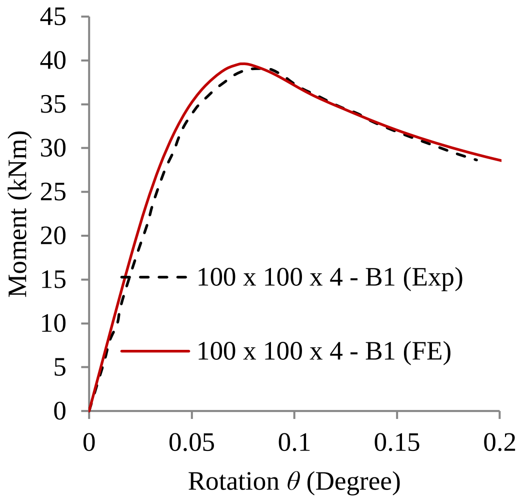

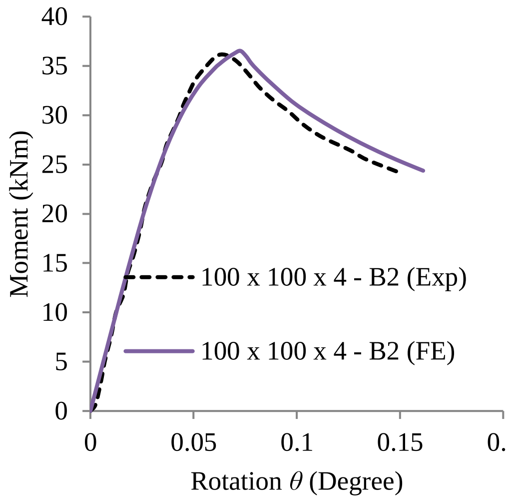

(g)

(h)

Fig. 4: Comparison of FE and experimental results of Theofanous and Gardner (2010) for LDSS square hollow beam.

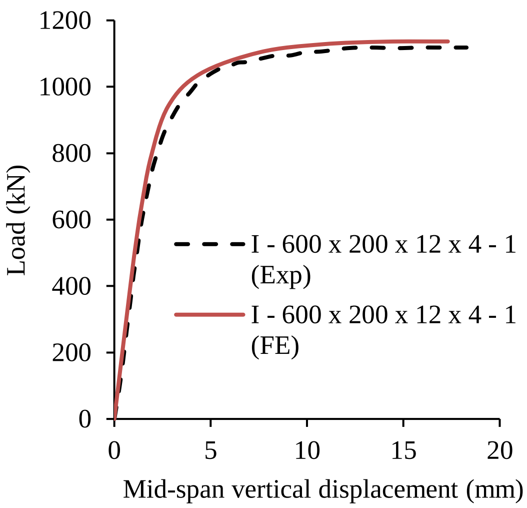

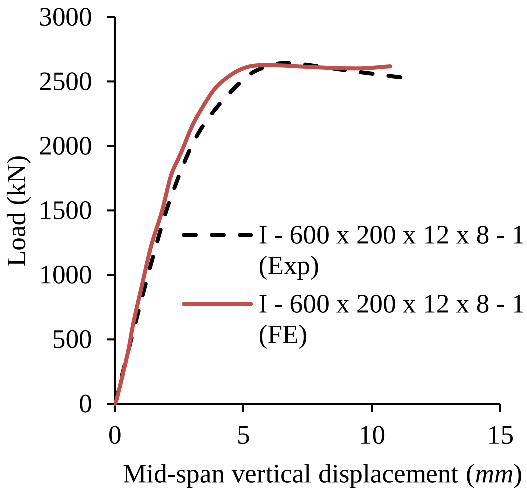

(a)

(b)

Fig. 5 Comparison of FE and experimental results of Saliba and Gardner (2013) for LDSS steel plate girders

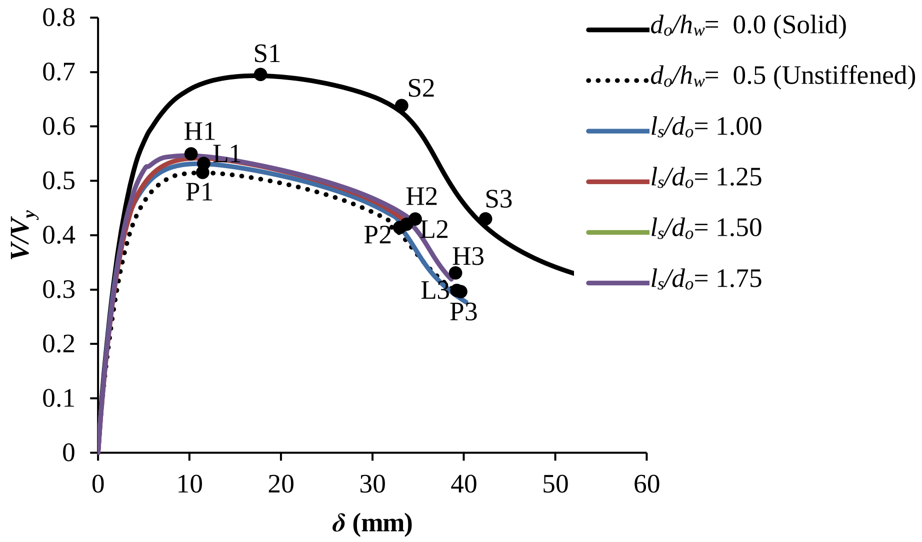

(a)

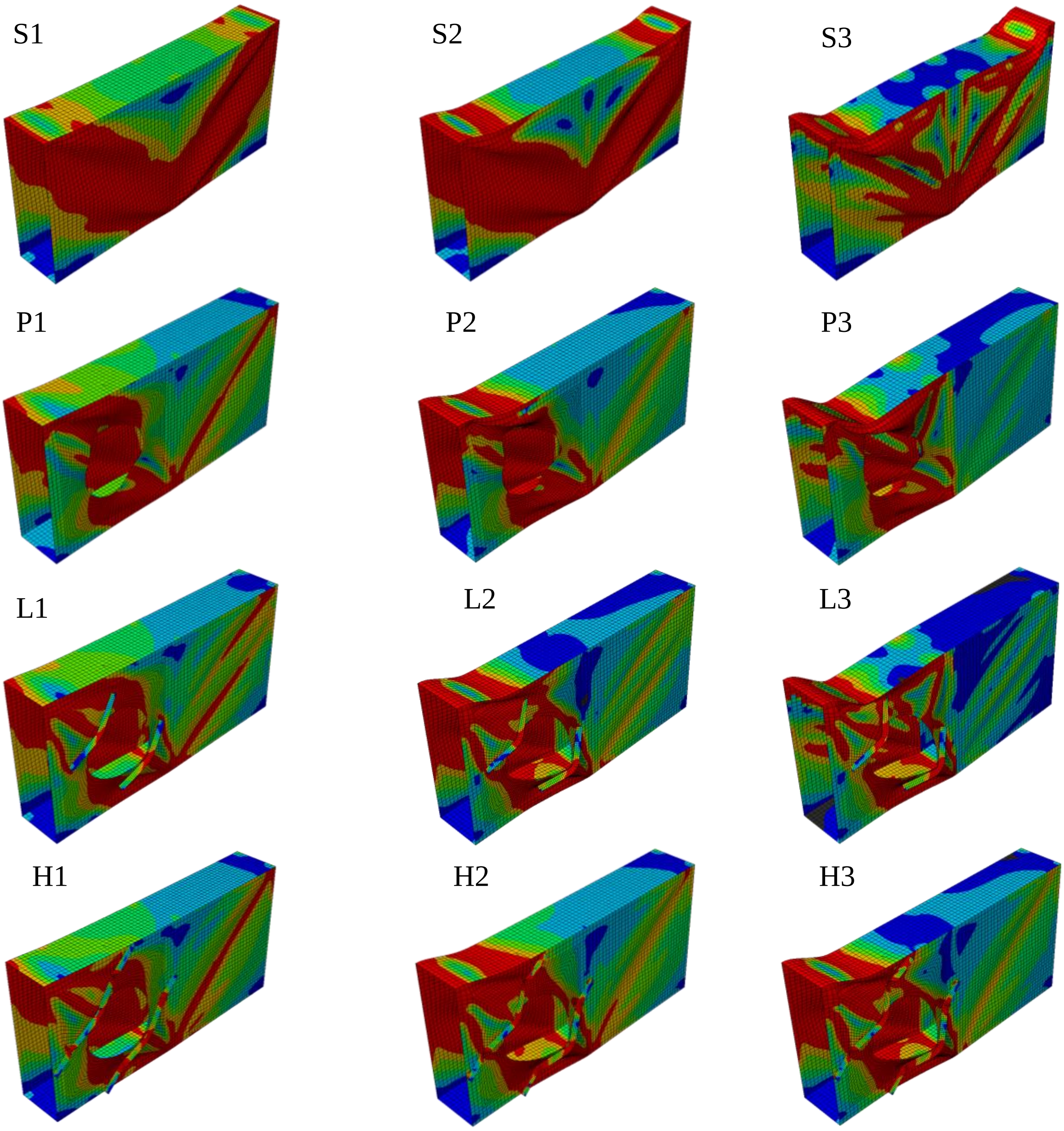

(b)

Fig. 6: (a) Variation of V/V_y vs δ (l_s/ d_o = 1.00–1.75, b_s/h_w = 0.04, t_s/t_w= 1)

(b) von-Mises stress contour for d_o/h_w = 0.0 (S1, S2, S3), d_o/h_w= 0.5 (P1, P2, P3) (x/h_w = 0.5, y/h_w = 0.5; a/h_w = 1.0, t_f/t_w =5), with l_s/d_o = 1.00 (L1, L2 & L3) & 1.75 (H1, H2 & H3) and t_s/t_w = 1.0.

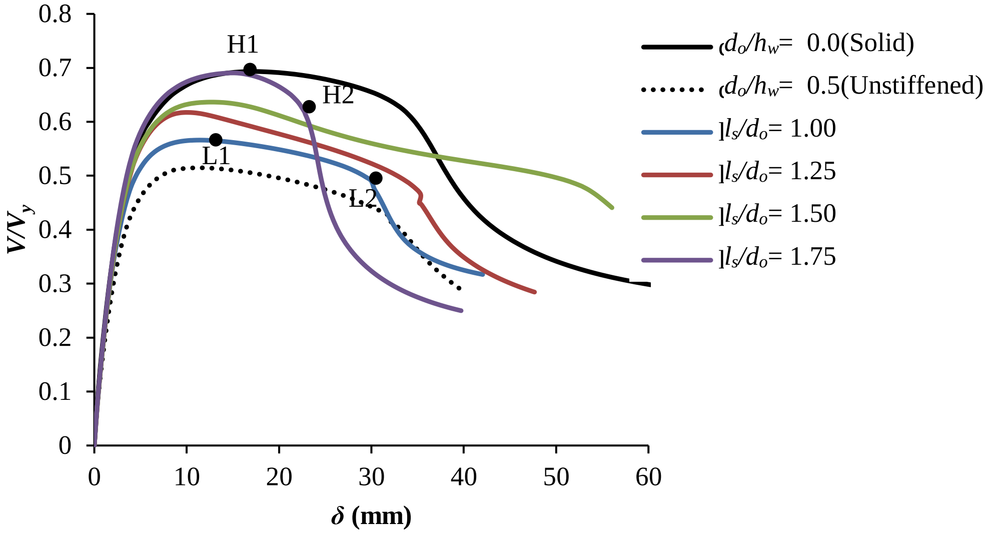

(a)

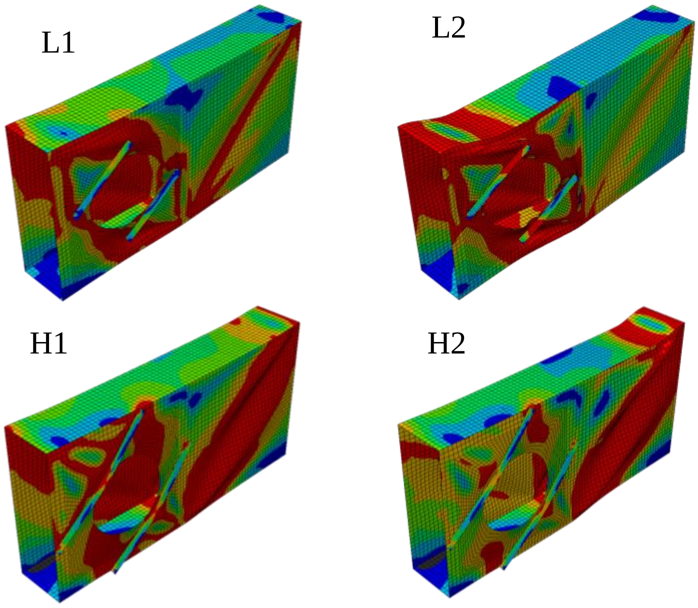

(b)

Fig. 7: (a) Variation of V/V_y vs δ (l_s/d_o = 1.00–1.75, b_s/h_w = 0.04, t_s/t_w= 7),

(b) von-Mises stress contour for l_s/d_o = 1.00 (L1 & L2) & l_s/d_o = 1.75 (H1 & H2)) and b_s/h_w= 0.04 (t_s/t_w = 7.0).

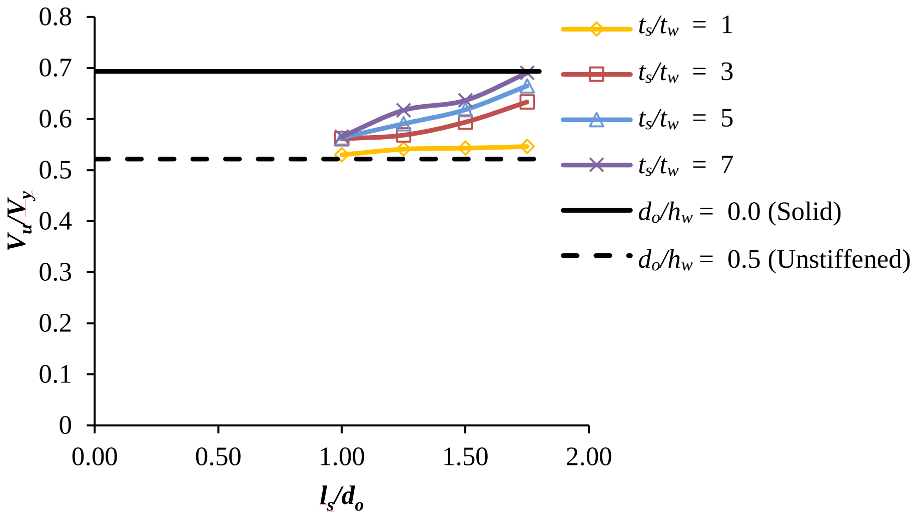

Fig. 8 **Variation of V_u/V_y with l_s/d_o (b_s/h_w = 0.04).**

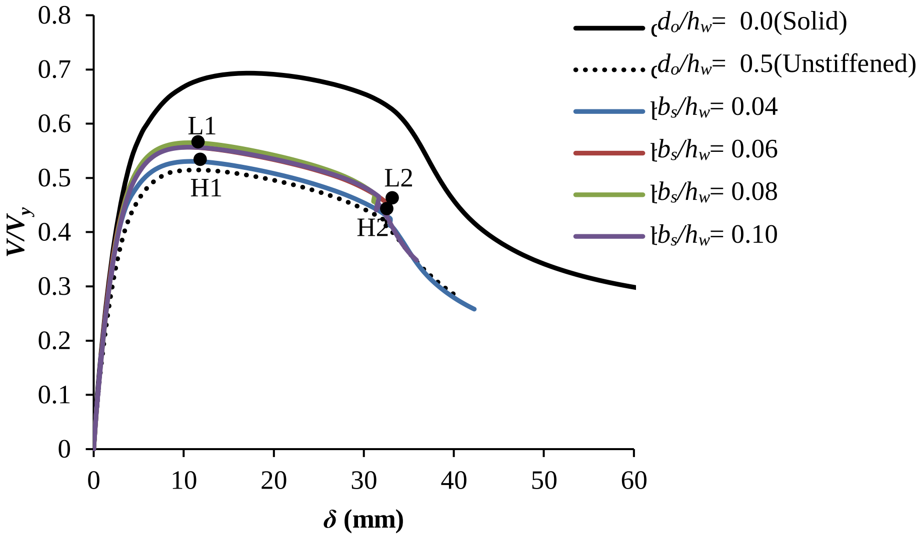

(a)

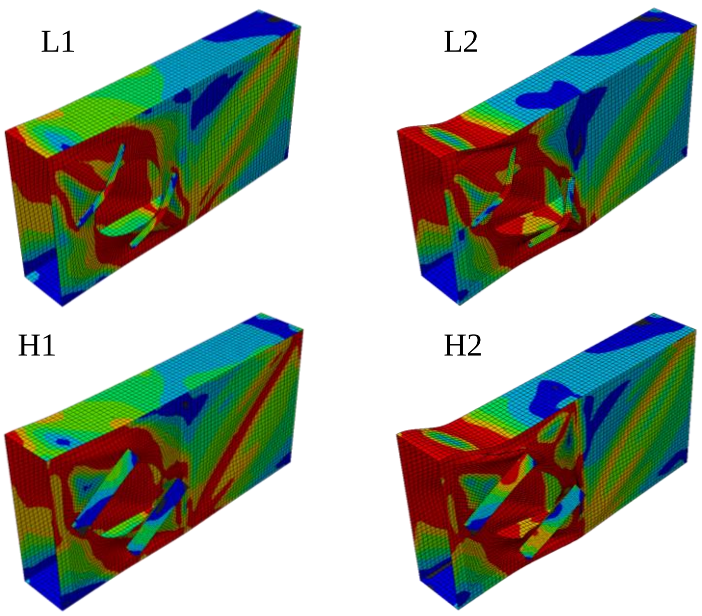

(b)

Fig. 9: **(a) Variation of V/V_y vs δ (b_s/h_w= 0.04–0.10, l_s/d_o = 1.00,t_s/t_w = 1.0),**

(b) von-Mises stress contour forb_s/h_w = 0.04 (L1 & L2) & 0.10 (H1 & H2) andl_s/d_o = 1.0 (t_s/t_w = 1.0)

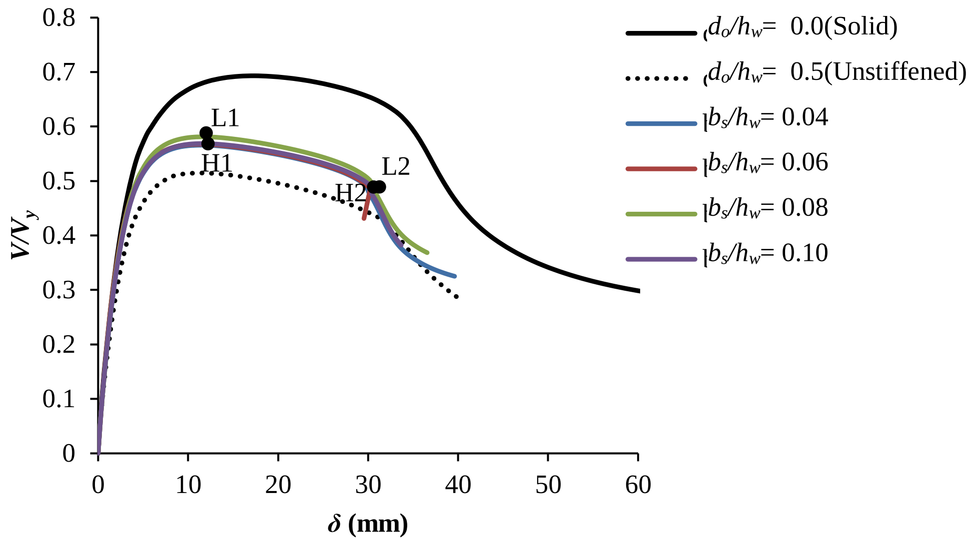

(a)

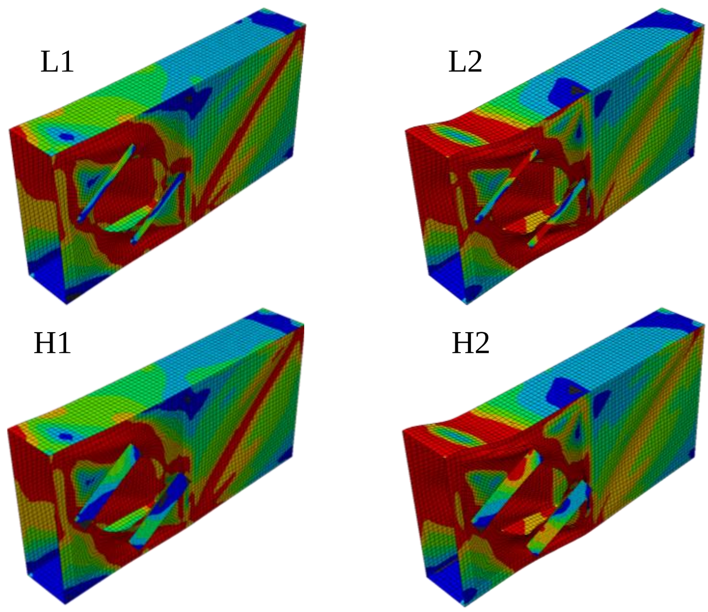

(b)

Fig. 10: (a) Variation of V/V_y vs δ (b_s/h_w= 0.04–0.10, l_s/d_o = 1.00,t_s/t_w = 7.0) of inclined flat stiffener,

(b) von-Mises stress contour forb_s/h_w = 0.04 (L1, L2 & L3) & 0.10 (H1, H2 & H3) andl_s/d_o = 1.0 (t_s/t_w = 7.0).

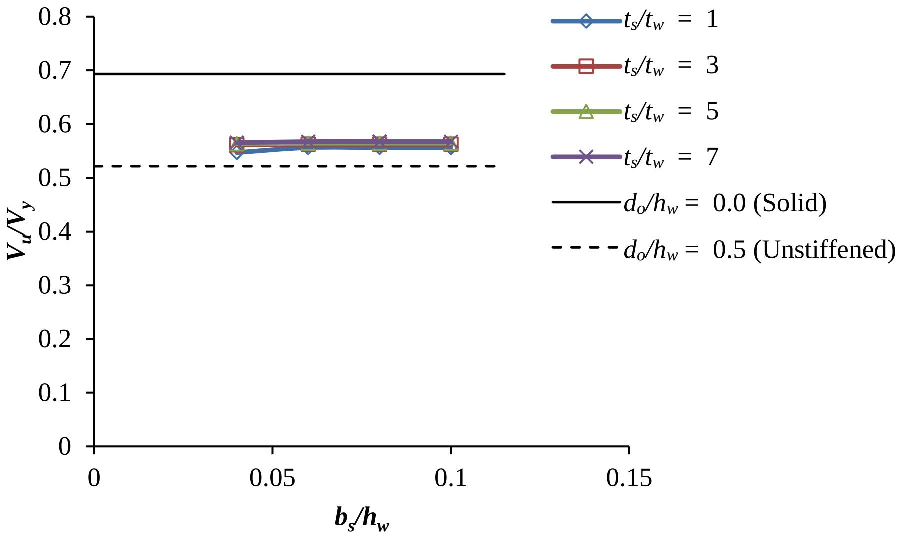

Fig. 11 Variation of V_u/V_y with b_s/h_w (l_s/d_o = 1.0)

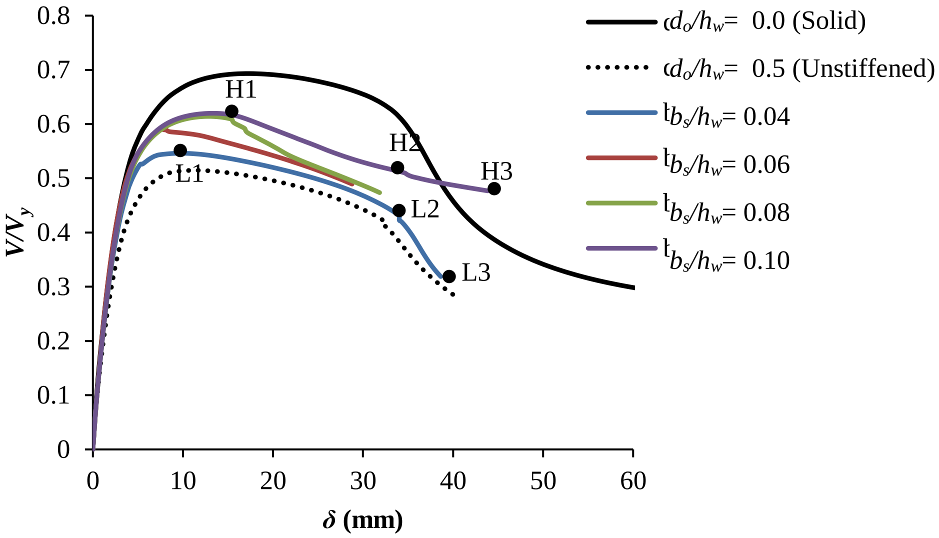

(a)

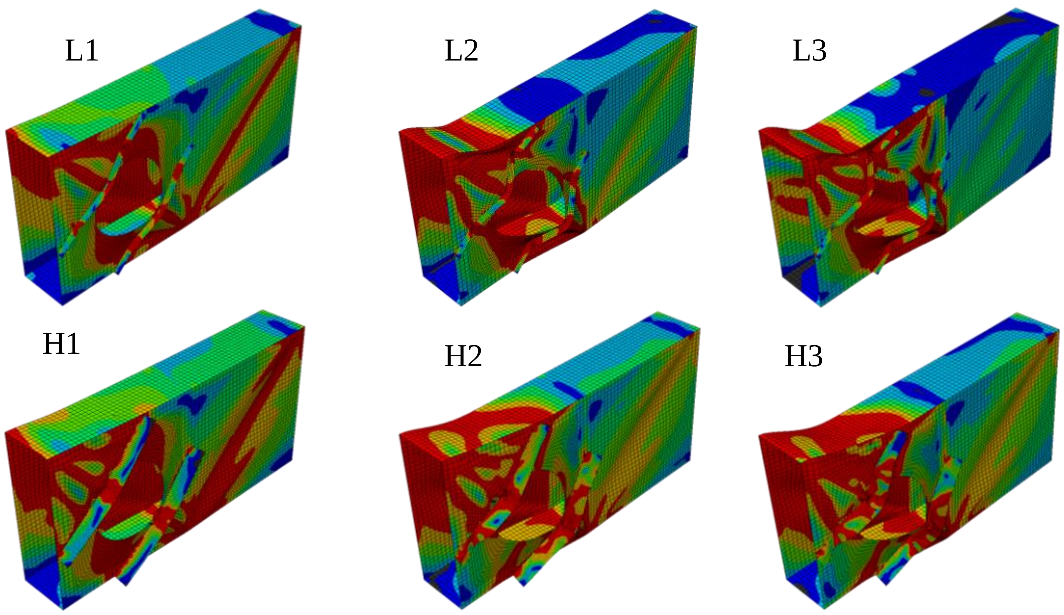

(b)

Fig. 12: (a) Variation of V/V_y vs δ (b_s/h_w= 0.04–0.10, l_s/d_o = 1.75, t_s/t_w= 1),

(b) von-Mises stress contour for b_s/h_w = 0.04 (L1, L2 & L3) & 0.10 (H1, H2 & H3) and l_s/d_o = 1.75 (t_s/t_w = 1.0).

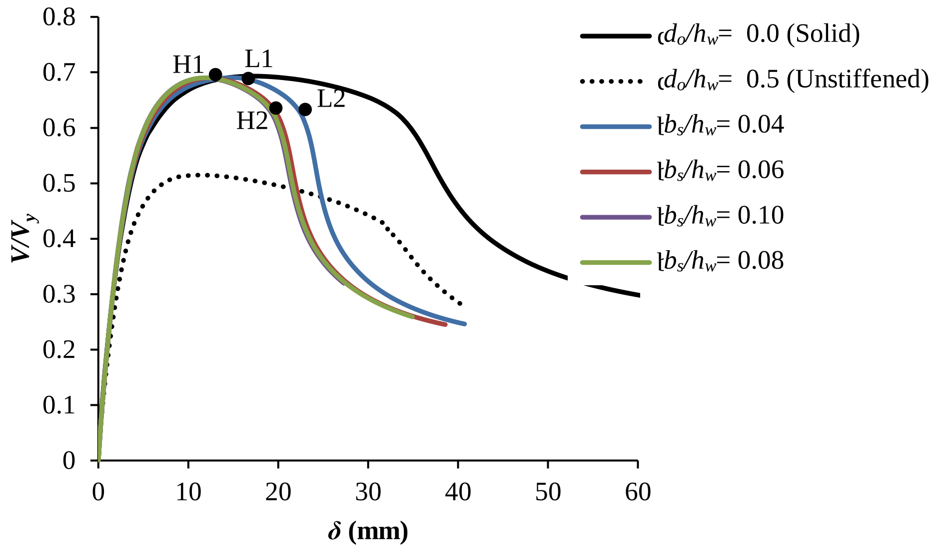

(a)

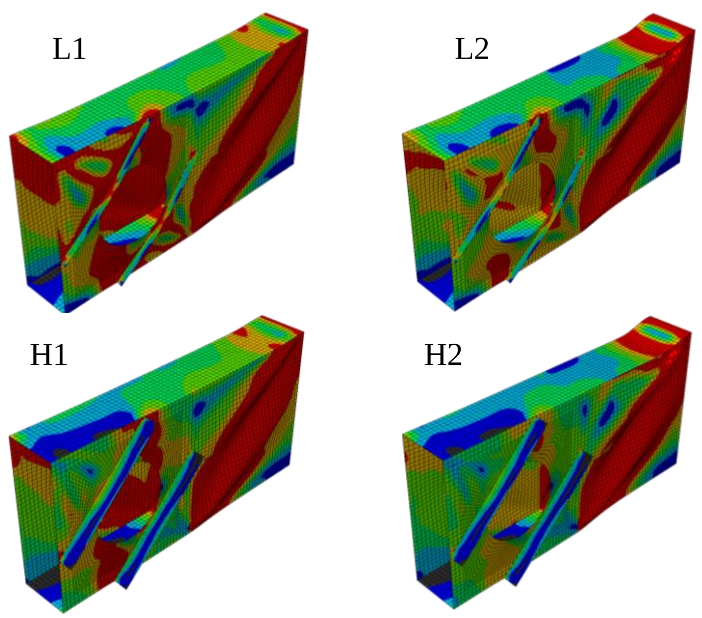

(b)

Fig. 13: (a) Variation of V/V_y vs δ (b_s/h_w= 0.04–0.10, l_s/d_o = 1.75, t_s/t_w= 7),

(b) von-Mises stress contour forb_s/h_w = 0.04 (L1 & L2) & 0.10 (H1 & H2) andl_s/d_o = 1.75 (t_s/t_w = 7.0).

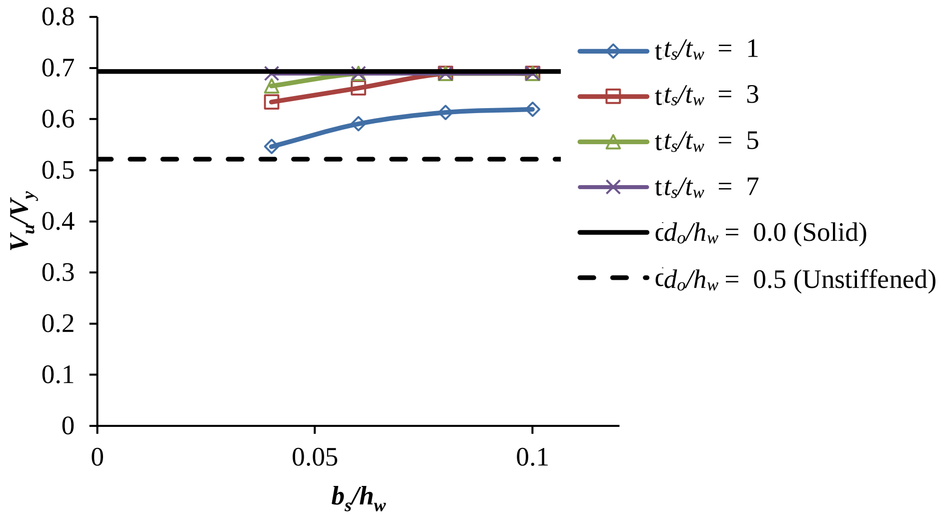

Fig. 14 Variation of V_u/V_y with b_s/h_w (l_s/d_o = 1.75).

7 Tables

Table 1 LDSS material properties (Theofanous and Gardner, 2010)

SHS 60 × 60 × 3 – B2 specimen					
a) Tension flat material properties					
E_o (MPa)	$\sigma_{0.2}$ (MPa)	$\sigma_{1.0}$ (MPa)	σ_u(MPa)	Compound R-O coefficients	
				n	$n'_{0.2,0.1}$
209797	755	819	839	6.0	4.3
b) Compression flat material properties					
206430	711	845	-	5.0	2.7
c) Tensile corner material properties					
212400	885	1024	1026	6.3	4.0

Table 2 LDSS square hollow beam dimensions (Theofanous and Gardner, 2010) for FE validation

Specimen	L (mm)	B (mm)	D (mm)	t (mm)	r_i(mm)	w_o
SHS 60x60x3-B2	1100	60	60	3.10	2.3	Eq. 1

L = Length, B = Width, H = Depth, t = thickness, r_i = internal corner radius, w_0 = local geometric imperfection

Table 3 LDSS Plate girders dimensions (Saliba and Gardner, 2013) for FE validation

Plate girder	L (mm)	a (mm)	e (mm)	h_w (mm)	b (mm)	t_f (mm)	t_w (mm)	t_s (mm)	b_s (mm)	a/h_w
I - 600 x 200 x 12 x 4 - 1	1360	600	80	598.8	200.1	12.4	4.1	20.9	98	1
I - 600 x 200 x 12 x 8 - 1	1360	600	80	600.3	200.1	12.5	8.2	20.6	96	1

L= specimen length, a = web panel length, e= distance between the end post andthe internal stiffener over the support, b= overall flange width,h_w =web depth, t_f = thickness of the flanges, t_w = thicknessof the web, b_s = (b -t_w)/2 is the width of the stiffeners and t_s = thickness of the stiffeners.

References

Abaqus., 2009. Hibbit, Karlsson, & Sorensen, Inc. Abaqus/Standard user's manual volumes 1-III and ABAQUS CAE manual. version 6.9-EF1, Pawtucket, USA.

Ashraf, M., Gardner, L. &Nethercot, D.A., 2006. Compression strength of stainless steel cross-sections, Journal of Constructional Steel Research; 62(1-2): 105-115.

Bowmick, A.K., 2014. Seismic behavior of steel plate shear walls with centrally placed circular perforations. Thin-Walled Structures; 75:30-42.

Cheng, B. & Li, C., 2012. Buckling Behavior of Strengthened Perforated Plates under Shear Loading. Steel and Composite Structures; 13 (4): 367-382.

Cheng, B. &Zhao, J., 2010. Strengthening of perforated plates under uniaxial compression: Buckling analysis. Thin-Walled Structures; 48 (12): 905-914.

Dawson, R.G. & Walker, A.C., 1972. Post-buckling of geometrically imperfect plates. Journal of the Structural Division, ASCE; 98: ST1:75-94.

Estrada, I., Real, E. &Mirambell, E., 2007. General behavior and effect of rigid and non-rigid end post in stainless steel plate girders loaded in shear. Part 1: Experimental study. Journal of Constructional Steel Research; 63 (7): 970-984.

Feng, R. & Young, B., 2015. Experimental investigation of aluminium alloy stub columns with circular openings. Journal of Structural Engineering; 141(11): 04015031.

Gardner, L., 2005. The use of stainless steel in structures. Progress in Structural Engineering and Materials; 7 (2): 45–55.

Gardner, L. & Ashraf, M. 2006. Structural design for non-linear metallic materials. Engineering Structures; 28(6):926–934.

Gardner, L. &Nethercot, D.A., 2004. Numerical Modeling of Stainless Steel Structural Components-A Consistent Approach. Journal of Structural Engineering; 130(10): 1586-1601.

Gardner, L., Saari, N. & Wang, F., 2010. Comparative experimental study of hot-rolled and cold-formed rectangular hollow sections. Thin-Walled Structures; 48(7): 495–507.

Hagen N.R., 2005. On the shear capacity of steel plate girders with large openings. PhD Thesis. Department of Structural Engineering. Faculty of Engineering Science. Norwegian University of science and technology.

Hagen, N.C., Larsen, P.K. &Alberg, A., 2009. Shear capacity of steel plate girders with large web openings, part 1: Modeling and simulations. Journal of Constructional Steel; 65(1): 142-150.

Hamoodi, M.J. &Gabar, M.S.A., 2013. Behavior of Steel Plate Girders with Web Openings Loaded in Shear. Engineering and Technical Journal; 31(15):2982-2995.

Huang, Y. & Young, B., 2013. Experimental and numerical investigation of cold-formed lean duplex stainless steel flexural members. Thin-Walled Structures; 73: 216–228.

Huang, Y. & Young, B., 2014. Structural performance of cold-formed lean duplex stainless steel columns. Thin-Walled Structures;83:59–69.

Keerthan, P. &Mahendran, M., 2013. Suitable stiffening systems for LiteSteel beams with web openings subjected to shear. Journal of Constructional Steel Research; 80: 412-428.

Kim, J.H., Jeon, J.H., Park, J.S., Seo, H.D., Ahn, H.J. & Lee, J.M., 2015. Effect of reinforcement on buckling and ultimate strength of perforated plates. International Journal of Mechanical Sciences; 92: 194-205.

Lagaros, N.D., Psarras, L.D., Papadrakakis, M. &Panagiotou, G., 2008. Optimum design of steel structures with web opening. Engineering Structures; 30(9): 2528-2537.

Liu, T.C. &Chung, K.F., 2003. Steel beams with large web openings of various shapes and sizes; finite element investigation. Journal of Constructional steel research; 59(9): 1159-1176.

Mann, A.P., 1993. The structural use of stainless steel. Structural Engineering; 71(4): 60–69.

Narayanan, R. & Der-Avanessian, N.G.V., 1984. Elastic buckling of perforated plates under shear. Thin-Walled Structures (1); 2:51-73.

Nilsson, J.O., Chai. G, &Kivisäkk, U., 2008. Recent development of stainless steels. In: Proceedings of the sixth European stainless steel conference: 585–590.

Paik, J.K., 2007. Ultimate strength of perforated plates under edge shear loading, Thin-walled structures; 45:301–306.

Patton, M.L. & Singh, K.D., 2012. Numerical modeling of lean duplex stainless steel hollow columns of square, L-, T-, and +-shaped cross sections under pure axial compression. Thin-Walled Structures; 53: 1–8.

Pellegrino, C., Maiorana, E. & Modena, C., 2009. Linear and non-linear behaviour of steel plates with circular and rectangular holes under shear loading. Thin-Walled Structures; 47(6-7): 607-616.

Ramberg, W. & Osgood, W.R., 1943. Description of stress-strain curves by three parameters. Washington DC, USA: National Advisory Committee for Aeronautics; technical Note No. 902.

Ridley-Ellis, D.J., 2000. Rectangular Hollow sections with circular web openings-Fundemental behavior in torsion, bending and shear. Ph.D. thesis, University of Nottingham.

Riks, E., 1979. An incremental approach to the solution of snapping problems. International Journal of Solids and Structures; 15:529-51.

Saliba, N. & Gardner, L., 2013, Experimental study of the shear response of lean duplex stainless steel plate girders. Engineering Structures; 46: 375–391.

Sonu, J.K. & Singh, K.D., 2017a. Shear characteristics of Lean Duplex Stainless Steel (LDSS) rectangular hollow beams. Structures; 10: 13-29.

Sonu, J.K. & Singh, K.D., 2017b. Shear behavior of single perforated Lean Duplex Stainless Steel (LDSS) rectangular hollow beams. Thin-Walled structures; 119: 851-867.

Theofanous, M. & Gardner, L., 2010. Experimental and numerical studies of lean duplex stainless steel beams. Journal of constructional steel research; 66(6): 816-825.

Theofanous, M., Chan, T.M. & Gardner, L., 2009. Flexural behaviour of stainless steel oval hollow sections. Thin-Walled structures; 47(6-7): 776-787.